DOI: 10.13009/EUCASS2023-346
Aerospace Europe Conference 2023 – 10TH EUCASS – 9TH CEAS

Direct numerical simulation of sloshing and phase change in LH2 tanks

Leandro Germes Martinez[1], *Benjamin Duret*[1†], *Julien Reveillon*[1], *François-Xavier Demoulin*[1] *and Amauric Jarry*[2]
[1] *CORIA-UMR 6614 - Normandie Université, CNRS-Université et INSA de Rouen,*
Campus Universitaire du Madrillet, 76800 Saint Etienne du Rouvray, France
[2] *CNES - Direction Technique et Numérique, 75012 PARIS, France*
germesml@coria.fr · duret@coria.fr
[†]Corresponding author

Abstract

Better understanding the boil-off phenomenon is necessary to optimize the storage and transportation of cryogenic liquids, especially during space missions where the cryogenic tank is subjected to various stresses. Here, a numerical study of sloshing and boiling in LH2 tanks using direct numerical simulation is presented. A compressible formalism is retained to capture phase change and interface deformation in a confined two-phase environment. Our objective is to analyze the behavior of the boil off rate in a sloshed cryogenic tank. A significant increase of the boiling rate is observed compared to the static configuration with the same parameters.

1. Introduction

Transporting or storing liquid hydrogen (LH2) can cause significant issues in aerospace industries due to its tendency to slosh, especially in microgravity conditions. This has become a growing concern as LH2 is being explored as a potential energy vector in the transport industries. Numerous studies have been conducted on sloshing since the work of Abramson et al[1] who proposed analytical models for predicting sloshing in tanks with various geometries. However, there have been limited studies that address the sloshing of vaporizing/boiling cryogenic fluids: for instance, the work of Arndt et al.[2] (numerical simulation), Lacapere et al.[10] (experimental) and Seo et al.[18] (modelling).

Besides the forces exerted by the liquid on the tank's walls, sloshing induces changes in the thermodynamic behavior of the liquid, leading to significant pressure changes when phase change occurs. This phenomenon, called boil-off, may lead to a release of gaseous hydrogen during transportation to avoid the self-pressurization of the tank. The subsequent mass loss is considered one of the most severe drawbacks of this energy (Ustolin et al.[20]). Several factors can trigger, and increase the boil-off of LH2, including increased surface area due to sloshing and heat flux entering through the walls.

These reasons prompted us to investigate this phenomenon using our in-house Direct Numerical Simulation (DNS) code ARCHER. In this work, the mass-conservative interface capturing (Coupled Level Set/Volume Of Fluid) method is adapted to account for the liquid mass variation due to phase change. In addition, the Stefan flow at the liquid/gas interface, acoustic effects, and the thermal dilatation of both phases can be captured. Furthermore, the method can handle several gas structures captured inside the liquid, each with independent temperature, density, and pressure. A detailed description of the system of equations solved, the implemented numerical methods, and their application can be found in our previous work (Germes et al.[11,12]).

In this work, a configuration of a half-filled LH2 container is simulated, where a sinusoidal acceleration along the x-axis represents the sloshing. First, a comparison between simulation results and linear theory is presented for an academic sloshing configuration. Then, a validation case of a boiling droplet is performed and illustrate the accuracy and potential of our numerical method. Finally, a sloshed and a static LH2 tanks are simulated. Results about the temporal evolution of the surface area, boiling rate, temperature, and velocity field are described and analyzed. These results show the influence of sloshing on the boiling rate and the surface area compared to the static configuration.

2. Governing equations

Compressible two-phase flows composed of pure liquid and gaseous hydrogen are considered in our simulations. In addition, heat and mass transfer across the interface can occur. The system of equations solved for both phases is the

DOI: 10.13009/EUCASS2023-346

following:

$$\begin{cases} \dfrac{\partial \rho}{\partial t} + \boldsymbol{\nabla} \cdot (\rho \boldsymbol{u}) = 0 & \text{(1a)} \\ \dfrac{\partial \rho \boldsymbol{u}}{\partial t} + \boldsymbol{\nabla} \cdot (\rho \boldsymbol{u} \otimes \boldsymbol{u}) = -\boldsymbol{\nabla} P + \boldsymbol{\nabla} \cdot \left[2\mu \bar{\bar{\epsilon}} - \dfrac{2}{3} \mu \left(\boldsymbol{\nabla} \cdot \boldsymbol{u} \right) \bar{\bar{I}} \right] + \rho \boldsymbol{f_{vol}} & \text{(1b)} \\ \rho c_p \left(\dfrac{\partial T}{\partial t} + \boldsymbol{u} \cdot \boldsymbol{\nabla} T \right) = \boldsymbol{\nabla} \cdot (\lambda \boldsymbol{\nabla} T) + \alpha_T T \left(\dfrac{\partial P}{\partial t} + \boldsymbol{u} \cdot \boldsymbol{\nabla} P \right) & \text{(1c)} \end{cases}$$

where ρ, $\boldsymbol{u}$, and P are the density, velocity, and pressure, respectively. $\bar{\bar{I}}$ is the identity matrix, $\bar{\bar{\epsilon}} = \frac{1}{2}\left(\boldsymbol{\nabla u} + \boldsymbol{\nabla u}^T\right)$, μ the dynamic viscosity, T is the temperature, $\boldsymbol{f_{vol}}$ represents volumetric forces (such as gravity and sloshing) and α_T is the thermal dilatation coefficient. Thermophysical properties, such as the thermal conductivity (λ), and heat capacities (c_p), are considered constants.

To close the system of equations, equations of state for each phase are necessary since both phases are considered compressible. For the liquid, a correlation for compressed liquid is used:

$$\rho_l = \rho_s \left[1 - c \ln \frac{\beta + P}{\beta + P_s} \right]^{-1} \tag{2}$$

where ρ_s is the density at saturation temperature, P_s saturation pressure, β is a parameter which depend on the temperature, and c is a constant. In the gas phase, the ideal gas equation is used:

$$\rho_g = \frac{P M_g}{RT} \tag{3}$$

where R is the ideal gas constant and the gas molar mass (M_g).

To follow the spatial and temporal evolution of the pressure, an equation is obtained using the continuity and energy conservation equation:

$$\left(\frac{\partial P}{\partial t} + \boldsymbol{u} \cdot \boldsymbol{\nabla} P \right) = -\rho c^2 \boldsymbol{\nabla} \cdot \boldsymbol{u} + \frac{\alpha_T c^2}{c_p} \left(\boldsymbol{\nabla} \cdot (\lambda \boldsymbol{\nabla} T) \right) \tag{4}$$

where c is the speed of sound. Equation 4 has been used in previous works (Martinez et al.[11]), and similar approaches can be found in the literature (Caltagirone et al.[5] Fuster et al.,[8] and Duret et al.[6]).

To account for the phase change within our system, jump conditions at the interface must be carefully implemented. This guarantees the conservation of mass, momentum, and species at the interface:

$$[\boldsymbol{u}]_\Gamma = \dot{\omega} \left[\frac{1}{\rho} \right]_\Gamma \tag{5}$$

$$[P - \boldsymbol{n} \cdot (2\mu \bar{\bar{\epsilon}}) \cdot \boldsymbol{n}]_\Gamma = \sigma H - \dot{\omega}^2 \left[\frac{1}{\rho} \right]_\Gamma \tag{6}$$

$$[\lambda \nabla T]_\Gamma = -\dot{\omega} h_{lv} \tag{7}$$

where $[A]_\Gamma = A_l - A_g$ for a given variable A, σ is the surface tension, H is the mean curvature, $\dot{\omega}$ is the phase change rate and h_{lv} the latent heat.

3. Numerical methods

In the ARCHER code, the coupled level-set/volume of the fluid (CLSVOF) method for interface representation, initially proposed by Menard et al.[14] for incompressible fluids, has been adapted to handle compressible fluids and phase change. To this end, additional terms are included on the right-hand side of the liquid volume fraction (α_l) transport equation:

$$\frac{\partial \alpha_l}{\partial t} + \boldsymbol{\nabla} \cdot (\alpha_l \boldsymbol{u}) = \alpha_l (1 - \alpha_l) D + \alpha_l \boldsymbol{\nabla} \cdot \boldsymbol{u} - \frac{\dot{m}}{\rho_l} \tag{8}$$

where

$$D = \frac{1}{\rho_g} \frac{D\rho_g}{Dt} - \frac{1}{\rho_l} \frac{D\rho_l}{Dt}$$

represents the compressibility or dilatation of the fluid, with $\frac{D}{Dt}$, as the material derivative. $\dot{m} = \rho_l \Sigma \| \boldsymbol{s_d} \|$ is the volumetric evaporation rate. It is estimated using the interface regression speed $\left(\boldsymbol{s_d} = \frac{\dot{\omega}}{\rho_l} \boldsymbol{n} \right)$ and local surface density $\left(\Sigma = \frac{S_\Gamma}{V_{cell}} \right)$

DOI: 10.13009/EUCASS2023-346

where S_Γ is the local surface area computed after the PLIC reconstruction and V_{cell} is the volume of the grid cell. The level set function, denoted as ϕ, is utilized to calculate the geometrical characteristics of the interface. This includes determining the normals $\left(\boldsymbol{n} = \frac{\boldsymbol{\nabla}\phi}{|\boldsymbol{\nabla}\phi|}\right)$ and the curvature ($\kappa = -\boldsymbol{\nabla}\cdot\boldsymbol{n}$).

In this work, an Eulerian staggered grid is considered, where the velocities are defined on the faces of the cell, and the scalars (e.g., P, α_l, T) are located in the center of the cell. To compute the velocity and pressure field, a projection method is used to solve the momentum equation (eq. 1b). The method has been modified to manage compressible flows by employing the pressure equation (eq. 4). Moreover, the viscous and convective terms in eq. 1b are solved using numerical schemes similar to the ones originally proposed by Sussman et al.[19] and Rudman et al.[17] To consider the velocity jump (eq. 6), the distribution method proposed by Boyd et al.[4] has been implemented. This method add a redistributed volumetric source term in the Poisson equation. The method involves shifting the Stefan flow a few cells away from the interface into the gas side. Using this technique allows the use of a consistent mass and momentum advection scheme and remove the costly requirement of constructing a continuous liquid velocity field. Jump conditions for heat and mass transfer are represented with the Ghost Fluid Method (Gibou et al.[9]).

The temperature field is obtained by solving eq. 1c for each phase:

$$\frac{\partial T_l}{\partial t} + (\boldsymbol{u}\cdot\boldsymbol{\nabla})\,T_l = \frac{1}{\rho_l c_{pl}}\boldsymbol{\nabla}\cdot(\lambda_l\boldsymbol{\nabla}T_l) + \alpha_{T,l}T_l\left(\frac{DP}{Dt}\right) \tag{9}$$

$$\frac{\partial T_g}{\partial t} + (\boldsymbol{u}\cdot\boldsymbol{\nabla})\,T_g = \frac{1}{\rho_g c_{pg}}\boldsymbol{\nabla}\cdot\left(\lambda_g\boldsymbol{\nabla}T_g\right) + \alpha_{T,g}T_g\left(\frac{DP}{Dt}\right) \tag{10}$$

The variables T_l and T_g denote the temperature in the liquid and gas phases, respectively. Here, a 5th-order WENO scheme is implemented to discretize the convective term and a 2nd-order central difference scheme is used for the diffusion term. Furthermore, the energy jump condition at the interface is implicitly considered by imposing the saturation temperature at the interface. This temperature is determined by assuming thermodynamic equilibrium at the interface and utilizing the Clausius-Clapeyron relation. Moreover, to avoid numerical heating/cooling during the solution of the convective term of eq. 1c, the temperature of each phase is extrapolated linearly using Aslam's extension method.[3] Also, the evaporation rate is computed from eq. 7, using the normal gradient of the temperature at the interface:

$$\dot{\omega} = \frac{[\lambda\boldsymbol{\nabla}T]_\Gamma}{h_{lv}} \tag{11}$$

4. Results

4.1 Validation

4.1.1 Lateral isentropic sloshing

Similar to Rossi et al.[16] and Park et al.,[15] for the validation of the sloshing without heat and mass transfer, a simple two-phase system in a rectangular domain of side $L = 0.52\,m$ is employed (see Figure 1). The liquid and gas properties correspond to water and air, respectively. In addition, a periodic displacement of amplitude $A_1 = 5\times10^{-3}\,m$ is imposed in the x-direction. This correspond to a $a_x = A_1\psi^2\sin(\psi t)$ where $\psi = 2\pi f$ is the angular frequency, and the frequency $f = 1\,Hz$. For these conditions, analytical results for the interface elevation ($\zeta(x,t)$) can be obtained using the linear theory proposed by Faltinsen et al.:[7]

$$\zeta(x,t) = \zeta_1(x,t) + \zeta_2(x,t) \tag{12}$$

where

$$\zeta_1(x,t) = \frac{A_1}{g}\left(x\psi^2 + \sum_{n=0}^{\infty} C_n\psi\sin(k_n x)\right)\sin(\psi t) \tag{13a}$$

$$\zeta_2(x,t) = -\frac{A_1}{g}\sum_{n=0}^{\infty}\psi_n\left(C_n + \frac{H_n}{\psi^2}\right)\sin(k_n x)\sin(\psi_n t) \tag{13b}$$

Here, g is the gravity acceleration, $\psi_n = [gk_n\tanh(k_n h)]^{\frac{1}{2}}$ is the natural frequency, $k_n = \frac{2n+1}{L}\pi$ is the wavenumber, and the others coefficient are defined as

$$H_n = \psi^3\left(\frac{4}{L}\right)\left(\frac{(-1)^n}{k_n^2}\right)$$

$$C_n = \frac{H_n}{\psi_n^2 - \psi^2}$$

DOI: 10.13009/EUCASS2023-346

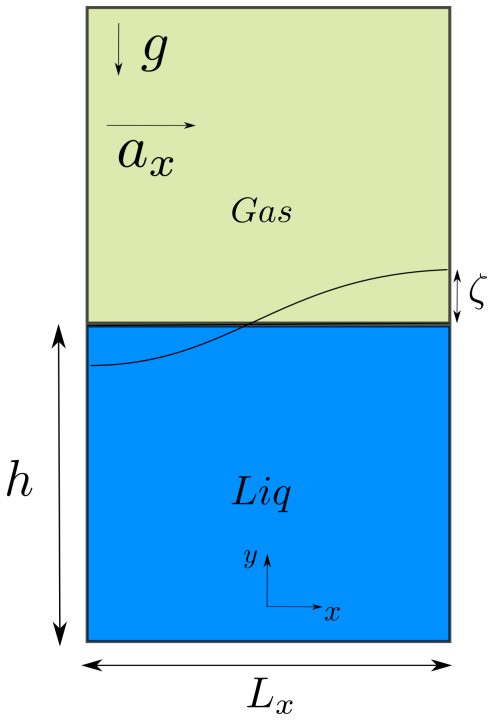

Figure 1: Numerical configuration of the lateral sloshing.

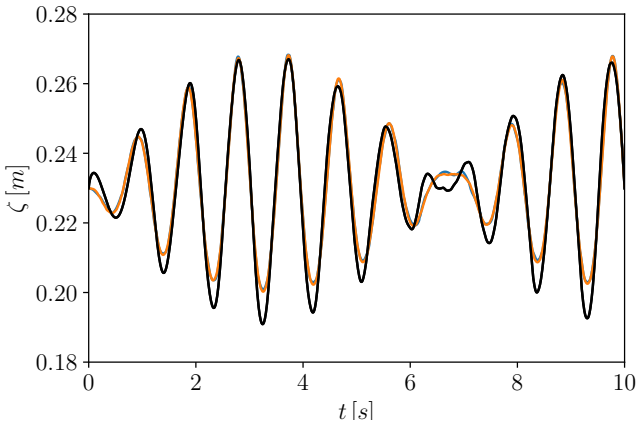

Figure 2: Temporal evolution of the interface level at the left side of the domain $\left(x = -\frac{L}{2}\right)$ resulted from the two simulations and the linear theory. Blue line: 64^2, orange line: 256^2, and black line: theory.

DOI: 10.13009/EUCASS2023-346

.

Two simulations were conducted, one with a mesh of 64^2 and the other with 256^2. Figure 2 shows the results of simulations and linear theory for the interface elevation over time. By comparing the frequency and maximal amplitudes, we can observe a good agreement with the theory. This indicates that the periodic lateral excitation has been implemented accurately and illustrates the capability of our method to recover the linear theory behavior.

4.1.2 Static boiling droplet

A 3D static droplet configuration is compared with the D^2 law to validate the implementation of the energy conservation equation and the jump conditions at the interface. According to this law, the square of the droplet diameter decreases linearly with time due to heat and mass transfer in the gas. To obtain the normalized squared radius equation, one must solve the continuity equation in spherical coordinates assuming a constant liquid mass flow $\left(\dot{m}' = 4\pi r^2 \rho \boldsymbol{u}\right)$ from the interface to the air :

$$\left(\frac{D_{th}}{D_0}\right)^2 = 1 - \frac{8K_d}{D_0^2}t \tag{14}$$

Table 1: Physical properties of the liquid phase and gas phase at the initial state for the static droplet simulations

	$\rho\left(kg\,m^{-3}\right)$	$\mu\left(kg\,m^{-1}s^{-1}\right)$	$\sigma\left(kg\,m^{-1}s^{-1}\right)$	$\lambda\left(W\,m^{-1}K^{-1}\right)$	$C_p\left(J\,kg^{-1}K^{-1}\right)$	$M\left(kg\,mol^{-1}\right)$	$h_{lv}\left(J\,kg^{-1}\right)$
Gas	1	1×10^{-5}	-	0.052	2000	29×10^{-3}	-
Liquid	700	3.26×10^{-4}	0.07	0.161	1000	18×10^{-3}	5.18×10^5

where $K_d = \frac{\rho_g}{\rho_l} D_{T,g} \log\left(1 + \frac{c_{p,g}(T_\infty - T_\Gamma)}{h_{lv}}\right)$ is the characteristic surface velocity regression, $D_{T,g} = \frac{\lambda_g}{\rho_g c_{p,g}}$ is the thermal diffusivity of the gas, T_∞ is the temperature far from the droplet and T_Γ is the temperature at the interface.

Similar to the configuration presented by Mialhe,[13] a static droplet with an initial radius of $R_D = 50\,\mu m$ suspended in its vapor is considered. The initial liquid temperature is $T_l = 329\,K$, and the initial gas temperature is $T_g = 700\,K$. The domain is a cube with a side length of $l_x = 4R_D$. The simulations are performed with three mesh sizes: 32^3, 48^3, and 64^3, and outflow boundary conditions are used in all directions. The liquid and gas have physical properties are summarized in table 1 for the initial state of the simulations. Figure 3(a) shows the temporal evolution of the square normalized diameter by the initial diameter of the droplet $\left(D^{*2} = \left(\frac{D}{D_0}\right)^2\right)$ obtained from the simulations and eq. 14. Here, a good agreement between the simulation results and the theory is observed. This demonstrates the ability of the code to describe accurately the thermal boundary layer close to the droplet surface. Also, it confirms that the coupling of the continuity, momentum, and energy conservation equation through the evaporation rate is properly implemented. In addition, a mesh convergence study is carried out by computing the L_p norms:

$$L_\infty = \max |D_{th}^{*2}(t) - D^{*2}(t)| \tag{15}$$

$$L_1 = \frac{\sum |D_{th}^{*2}(t) - D^{*2}(t)|}{N} \tag{16}$$

$$L_2 = \sqrt{\frac{\sum |D_{th}^{*2}(t) - D^{*2}(t)|^2}{N}} \tag{17}$$

The results are shown in Figure 3(b) and a mesh convergence of at least order 1 is obtained, showing the potential of the method to accurately represent boiling.

4.2 Boiling in a sloshed or static cryogenic tank

4.2.1 2D simulation

A compressible two-phase configuration with phase change is employed to study the pressure, heat transfer, and mass transfer in a cryogenics tank submitted to a sinusoidal lateral excitation. Simulations are carried out in a 2D rectangular domain with a length size $l_x = 8 \times 10^{-3}\,m$ and $l_y = 2l_x$, an initial liquid height $h = l_x$ and a mesh of 256×512. The liquid and gas have physical properties similar to those of hydrogen and are summarized in table 2 for the initial state of the simulations.

In this section, three different simulations were performed. First, the simulation of a cryogenic tank with heat and mass transfer with a sinusoidal lateral acceleration computed as

$$a_x = A_2 \sin(\psi t)$$

DOI: 10.13009/EUCASS2023-346

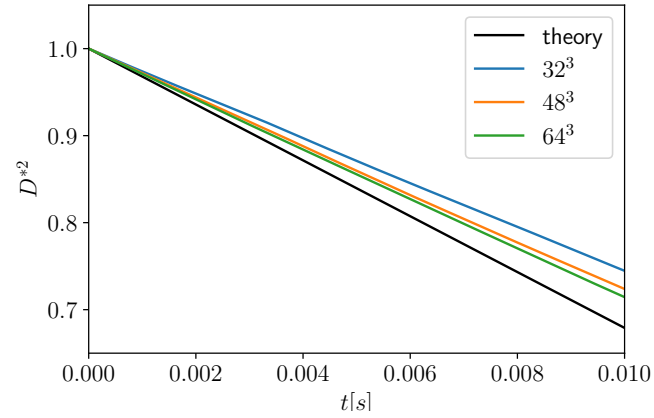

(a)

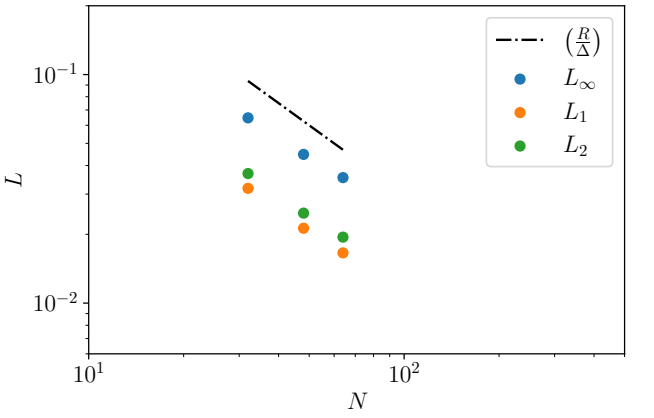

(b)

Figure 3: Static boiling droplet: a) Temporal evolution of the normalized square diameter; b) L_∞, L_1 and L_2 norms of the normalized square diameter.

Table 2: Physical properties of the liquid phase and gas phase at the initial state of the simulations

	$\rho\left(kg\,m^{-3}\right)$	$\mu\left(kg\,m^{-1}\,s^{-1}\right)$	$\sigma\left(kg\,m^{-1}\,s^{-1}\right)$	$\lambda\left(W\,m^{-1}K^{-1}\right)$	$C_p\left(J\,kg^{-1}K^{-1}\right)$	$M\left(kg\,mol^{-1}\right)$	$h_{lv}\left(J\,kg^{-1}\right)$
Gas	1.3	9.758×10^{-7}	-	0.017	11892	0.002	-
Liquid	71	1.391×10^{-5}	0.001	0.104	9569	0.002	4.5×10^5

where $A_2 = 2\|\boldsymbol{g}\|$ is the maximal amplitude, and $f = 20.98Hz$. This supplementary term is added as a volumetrical force to the RHS of the momentum equation, similar to the gravitational force. The initial liquid temperature is $T_l = 21K$, and the initial gas temperature is $T_g = 31K$. Also, no-slip boundary conditions are used in all directions for the velocity field. Regarding the temperature boundary conditions, we consider the bottom of the domain isolated, while assuming a constant heat flux of $\phi = 50\ Wm^{-1}$ for the remaining directions. In Figure 4, we can see the temperature field (Figures 4(a) and 4(c)) and the velocity field (Figures 4(b) and 4(d)) for $t^* = 5$ and $t^* = 10$, with the interface represented by the level-set function. Furthermore, it shows how the sloshing influence the liquid-gas interface: entrapped gas, fragmentation, and wrinkling can be observed. The transport of temperature due to the velocity field is also directly illustrated.

Moreover, a second simulation use the same set of parameters and perturbation amplitude as the first one, but the heat and mass transfer has been turned off (isentropic configuration). This allows us to analyze the effects of phase change in the interface transport and fluid dynamic behavior. Figure 5 shows the temporal evolution of the interface density ($\overline{\Sigma} = \frac{S_L}{V}$) where S_L is the total surface computed after the PLIC (Piecewise linear interface calculation) reconstruction, and V is the volume of the domain. In Figure 5, $t^* = \frac{t}{T_{period}}$ is the time normalized by the period of the

DOI: 10.13009/EUCASS2023-346

perturbation, the blue line corresponds to the first simulation, and the black line corresponds to the second simulation. From our observations, we noticed that the interface density's order of magnitude is comparable in both simulations. However, the main difference between the two is that the isentropic simulation exhibits less wrinkling or fragmentation of the interface at the beginning of the simulation compared to the simulation with boiling. It is expected since the introduction of heat and mass transfer has a direct influence of the density, which are computed through the equation of state in both phases. Consequently, the $\rho \boldsymbol{u}$ terms in the momentum equation should be different, especially close to the interface and then influence its behavior.

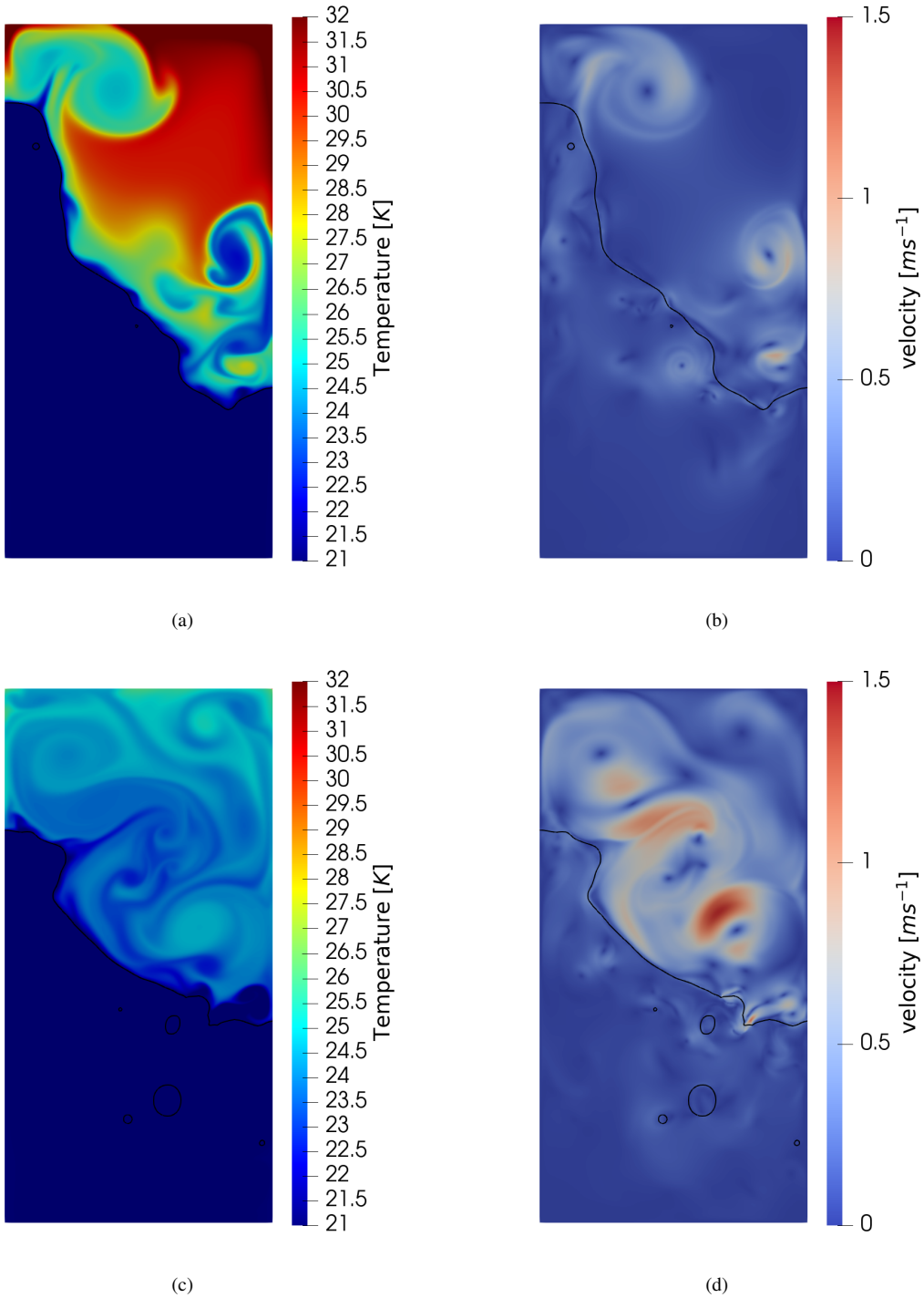

Figure 4: Sloshing in a cryogenic tank: a) Temperature field and b) velocity field with interface representation at $t^* = 5$, and c) Temperature field and d) velocity field with interface representation at $t^* = 10$.

DOI: 10.13009/EUCASS2023-346

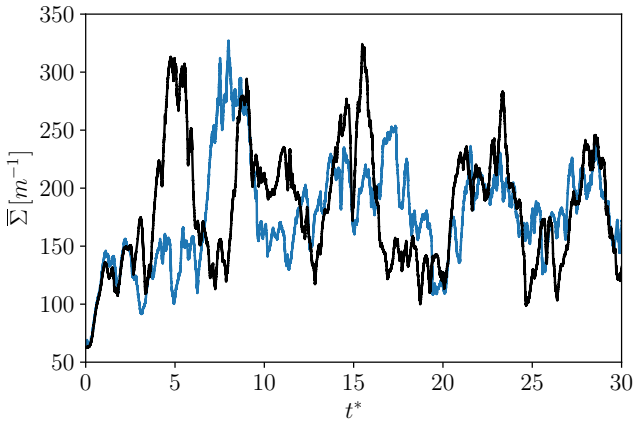

Figure 5: Temporal evolution of the interface density. Blue line: sloshing simulation with boiling; black line: isentropic simulation.

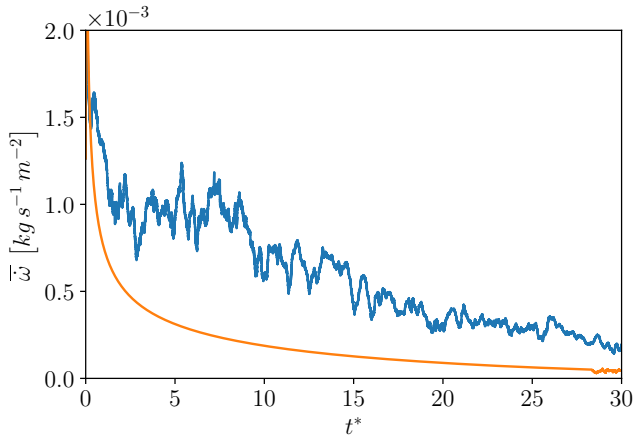

Figure 6: Temporal evolution of the phase change rate. Blue line: sloshing simulation with boiling; orange line: static simulation.

The third simulation shares the same characteristic as the first, but without any sloshing. The purpose of this is to analyze how interface deformation affects the phase change rate and pressure over time. In Figure 6, the temporal evolution of the surface mean of the evaporation rate $\left(\overline{\dot{\omega}} = \frac{1}{S}\int \dot{\omega} dS\right)$ for the simulation with and without sloshing is compared. Here, the blue line corresponds to the simulation with sloshing, and the orange line corresponds to the static stimulation. Many observations can be made, such as the boiling rate reaching its peak during the initial simulation stages because of the significant temperature gradients during initialization. In addition, the signal of the boiling rate obtained from the sloshing simulation has more noise and higher values than the signal obtained with the static simulation. There are two main reasons for this phenomenon. First, the sloshing causes deformation of the interface, leading to a larger, and fluctuating, surface area (see Figure 5) where the phase change occurs. Second, the sloshing enhances the mixing between the two phases, cooling both phases and also feed the boiling rate through temperature gradient until $t^* = 10$. Finally, a change of behavior is observed when $t^* > 10$, the temperature is quasi equal in both phase, and only the effect of boiling remains and the boiling rate tends to a plateau.

Additionally, Figure 7 displays the temporal progression of the pressure normalized by its initial value, denoted as $\overline{Pr}^* = \frac{\overline{Pr}}{\overline{Pr}^0}$. During the static stimulation, there is a slight drop in pressure after the initialization of the simulation. However, it then progressively increases linearly for the duration of the simulation. On the other hand, in the sloshing simulation, there is a significant decrease of 12% in the initial pressure during the first ten periods of the perturbation signal. During this period, the pressure drop can be explained by the mixing (cooling of the gaseous phase) and higher rate of phase change. After $t^* = 10$, the available energy seems to be only used for boiling (latent heat) compared to sensible heat, since the temperature of both phase is quasi equal ($< 1K$ difference). The boiling increases the pressure of the system. Consequently, two different pressure behavior can be observed if the tank is static or sloshed.

DOI: 10.13009/EUCASS2023-346

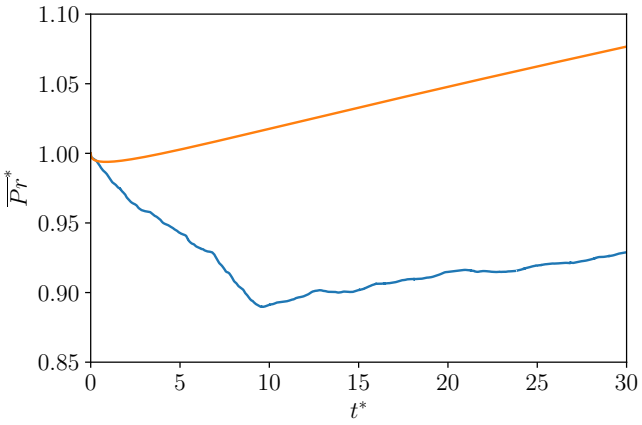

Figure 7: Temporal evolution of the phase change rate. Blue line: sloshing simulation with boiling; orange line: static simulation.

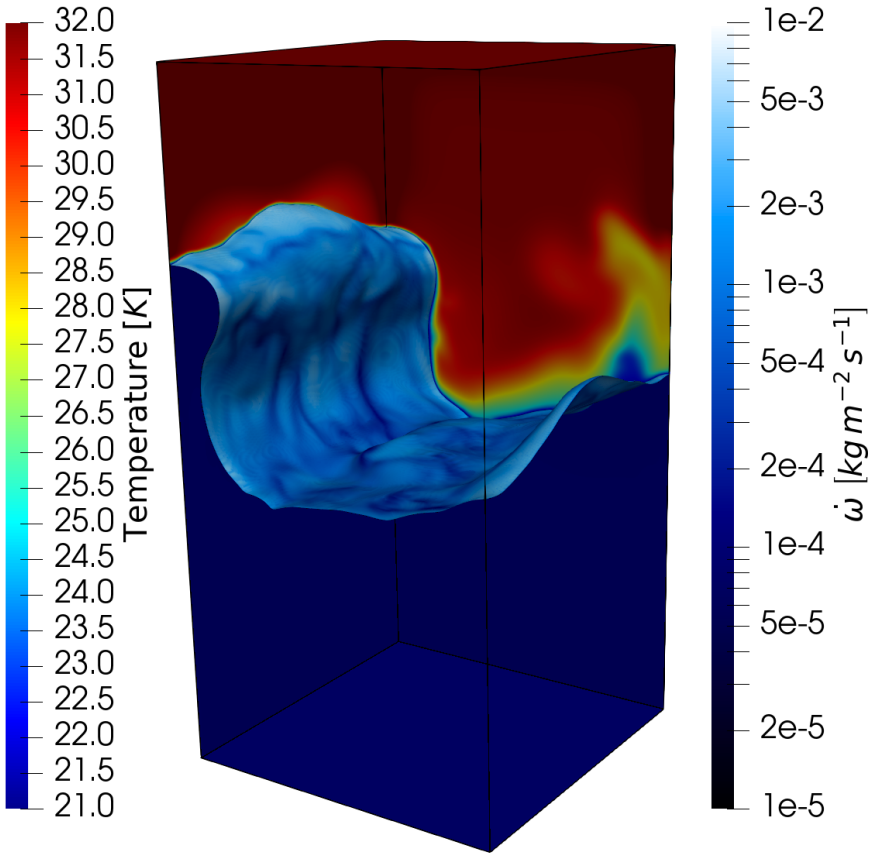

Figure 8: Temperature field in the 3D configuration on the boundary of the domain and visualization of the boiling rate at the interface.

4.2.2 3D simulation

Since turbulence and interface behavior tends to be quite different in three dimensional cases, additional 3D configurations are investigated with similar parameters. A first result is illustrated in Figure 8, showing the potential of our method to capture phase change and the interface topology. 3D computations are very expensive when phase change is taken into account and, as such, couldn't be incorporated in this full paper. However, 3D results will be shown during the EUCASS conference.

DOI: 10.13009/EUCASS2023-346

5. Conclusion

Direct numerical simulations of compressible two phase flows are used to investigate heat and mass transfer in a sloshing cryogenic tank containing pure liquid and gaseous hydrogen. This approach allows us to account for many physical phenomena such as thermal dilatation, interface deformation/fragmentation, natural convection and changes in velocity due to phase change in an enclosed environment without relying on any models. A two-phase sloshing configuration and a D^2 law configuration for a static boiling droplet have been used to validate the numerical formalism.

A detailed analysis is conducted on the interface behavior, boiling rate, and pressure temporal evolution in static and sloshed configurations. The results indicate that the evaporation process plays a crucial role in the pressure temporal evolution. Furthermore, the study highlights the impact of sloshing on the behavior of the pressure field. These insights demonstrate the potential of our ARCHER code to quantify the boiling rate and the self-pressurization of cryogenic tanks, whether in gravity or micro-gravity conditions.

6. Acknowledgments

This work was granted access to the HPC resources of IDRIS, TGCC, and CINES under the allocation (A0132B10101) made by GENCI (Grand Equipement National de Calcul Intensif). The CRIANN (Centre Regional Informatique et d'Applications Numeriques de Normandie) is also gratefully acknowledged (project No. 2017004) for its CPU resources. This research has been founded by the ANR agency (Agence Nationale de la Recherche), project number ANR-21-CE05-0010.

References

[1] H Norman Abramson. The dynamic behavior of liquids in moving containers, with applications to space vehicle technology. Technical report, 1966.

[2] Tim Arndt, Michael Dreyer, Philipp Behruzi, Mike Winter, and Arnold vanForeest. Cryogenic sloshing tests in a pressurized cylindrical reservoir. In *45th AIAA/ASME/SAE/ASEE joint propulsion conference & exhibit*, page 4860, 2009.

[3] Tariq D Aslam. A partial differential equation approach to multidimensional extrapolation. *Journal of Computational Physics*, 193(1):349–355, 2004.

[4] Bradley Boyd and Yue Ling. A consistent volume-of-fluid approach for direct numerical simulation of the aerodynamic breakup of a vaporizing drop. *Computers & Fluids*, 254:105807, 2023.

[5] Jean-Paul Caltagirone, Stéphane Vincent, and Céline Caruyer. A multiphase compressible model for the simulation of multiphase flows. *Computers & fluids*, 50(1):24–34, 2011.

[6] Benjamin Duret, R Canu, J Reveillon, and FX Demoulin. A pressure based method for vaporizing compressible two-phase flows with interface capturing approach. *International Journal of Multiphase Flow*, 108:42–50, 2018.

[7] Odd M Faltinsen. A numerical nonlinear method of sloshing in tanks with two-dimensional flow. *Journal of Ship Research*, 22(03):193–202, 1978.

[8] Daniel Fuster and Stéphane Popinet. An all-mach method for the simulation of bubble dynamics problems in the presence of surface tension. *Journal of Computational Physics*, 374:752–768, 2018.

[9] Frédéric Gibou, Liguo Chen, Duc Nguyen, and Sanjoy Banerjee. A level set based sharp interface method for the multiphase incompressible navier–stokes equations with phase change. *Journal of Computational Physics*, 222(2):536–555, 2007.

[10] Jerome Lacapere, B Vieille, and Benjamin Legrand. Experimental and numerical results of sloshing with cryogenic fluids. *Progress in Propulsion Physics*, 1:267–278, 2009.

[11] L Germes Martinez, Benjamin Duret, J Reveillon, and FX Demoulin. A new dns formalism dedicated to turbulent two-phase flows with phase change. *International Journal of Multiphase Flow*, 143:103762, 2021.

[12] L Germes Martinez, Benjamin Duret, J Reveillon, and FX Demoulin. Vapor mixing in turbulent vaporizing flows. *International Journal of Multiphase Flow*, page 104388, 2023.

DOI: 10.13009/EUCASS2023-346

[13] Guillaume Mialhe. *Simulation numérique directe de l'évaporation d'une goutte en interaction avec une paroi surchauffée*. PhD thesis, Université Toulouse 3 - Paul Sabatier, 2022.

[14] T. Ménard, S. Tanguy, and A. Berlemont. Coupling level set/VOF/ghost fluid methods: Validation and application to 3d simulation of the primary break-up of a liquid jet. *International Journal of Multiphase Flow*, 33(5):510–524, May 2007.

[15] Won Man Park, Dae Kyung Choi, Kyungsoo Kim, Sung Man Son, Se Hong Oh, Kang Hee Lee, Heung Seok Kang, and Choengryul Choi. Simple analytical method for predicting the sloshing motion in a rectangular pool. *Nuclear Engineering and Technology*, 52(5):947–955, 2020.

[16] Daniele Rossi, Davide Ubaldini, Simone Di Giorgio, and Sergio Pirozzoli. Navier–stokes simulations of vertical sloshing with time-periodic excitation. *International Journal of Multiphase Flow*, page 104505, 2023.

[17] Murray Rudman. A volume-tracking method for incompressible multifluid flows with large density variations. *International Journal for Numerical Methods in Fluids*, 28(2):357–378, August 1998.

[18] Mansu Seo and Sangkwon Jeong. Analysis of self-pressurization phenomenon of cryogenic fluid storage tank with thermal diffusion model. *Cryogenics*, 50(9):549–555, 2010.

[19] Mark Sussman and Elbridge Gerry Puckett. A coupled level set and volume-of-fluid method for computing 3d and axisymmetric incompressible two-phase flows. *Journal of computational physics*, 162(2):301–337, 2000.

[20] Federico Ustolin, Nicola Paltrinieri, and Filippo Berto. Loss of integrity of hydrogen technologies: A critical review. *international journal of hydrogen energy*, 45(43):23809–23840, 2020.